Silicon Nanocluster Anion-Argon Cation Recombination via Hybrid Continuum-Molecular Dynamics Calculations

Tomoya Tamadate & Christopher J. Hogan Jr.*

Department of Mechanical Engineering, University of Minnesota, Minneapolis, MN, USA

Submitted to:

Journal of Aerosol Science

^{*}To whom correspondence should be addressed: CJH: hogan108@umn.edu

ABSTRACT

Prediction of the charge distribution on particles in an aerosol is critical not only in electrical mobility based characterization methods, but also in understanding the role that charging plays in particle growth in gas phase synthesis reactors. The latter is particularly important in non-thermal plasma synthesis reactors, wherein nanoclusters form and grow from vapor phase precursors in a high electron and high ion density environment. In plasmas, because free electrons are much less massive and much more mobile than positive gas ions, nanocluster However, neutral or even positively charged charge distributions are biased negative. nanoclusters may exist, depending on the rate of nanocluster-gas ion recombination, and nanocluster-nanocluster collisions may greatly contribute to nanocluster growth if not Coulombically suppressed. To better understand the charge distribution on nanoclusters in nonthermal plasma synthesis systems, we applied a recently developed collision rate calculation method, i.e. the continuum-molecular dynamics (C-MD) method, to examine recombination of Si_n^z nanoclusters (n = 47,91,266, & 494, z = -1, & -2) and Ar^+ cations at 300 K and pressures from $10^{3.5} - 10^6$ Pa, in argon neutral gas. With collision rate coefficients from the C-MD approach, nanocluster steady-state charge distributions were calculated. C-MD determined recombination rate coefficients are found to be higher than those from the traditionally-used limiting sphere theory approach of Fuchs outside of the continuum limit, leading to charge distributions which, although biased towards negative charge levels, are less biased than predicted by the traditional limiting sphere method, with differences particularly noticeable at Application of C-MD recombination coefficients in steady-state charge lower pressures. distribution calculations shows that the fraction of positively charged nanoclusters in a nonthermal plasma would be negligibly small; however, there is an appreciable fraction of neutral nanoclusters, and hence nanocluster-nanocluster collisions cannot be neglected in modeling particle growth in plasma reactors.

1. INTRODUCTION

Understanding the charge distribution on nanoclusters (nanometer scale species composed of 10⁰-10² atoms) in aerosol and plasma synthesis reactors is important in mobility-based measurements of size distributions, as well as in understanding the role the ionization plays in nanoparticle nucleation and growth (Adachi *et al.*, 1985; Gopalakrishnan *et al.*, 2015). In large part, nanocluster charge distributions are controlled by diffusion charging, i.e. the collision of ions and electrons with nanoclusters, with charge transfer from the ion or electron to the condensed nanoclusters assumed (because the nanocluster is much more massive than the ion). With collision rates known and ionized species densities known, charge distribution calculation simply requires solution to a system of differential equations (Marlow & Brock, 1975).

Collision rate calculation for nanoclusters and ionized species in aerosols and plasmas, however, remains a challenge. In diffusion charging, collisions can be divided up into three broad classes: (1) collisions between a neutral nanocluster and ion or electron, (2) collisions between a like-charged nanocluster and ion or electron (e.g. a negatively charged nanocluster and electron), or (3) collisions between an unlike-charged nanocluster and ion or electron (e.g. a negatively charged nanocluster and positive ion, commonly termed ion-ion recombination (Natanson, 1960)). The collision rate in cases (1) and (2) is rather well-described by existing theories; in atmospheric pressure or reduced pressure systems, free molecular (collisionless) models accurately describe collision rates considering potential interactions between colliding species (Mott-Smith & Langmuir, 1926; Allen, 1992). However, difficulties in calculating the collision rate for case (3) still persist today, despite interest in ion-ion recombination for well over 100 years (Langevin, 1903; Thomson, 1924; Loeb & Marshall, 1929; Loeb, 1937). The

colliding species are significantly smaller in size than their persistence distances, hence at first it would seem that free molecular calculation approaches should apply (also called mean free paths) (Fuchs, 1963; Dahneke, 1983)). However, the distance over which they interact is governed by electrostatics, and is not necessarily small in comparison to persistence distances. Thus, a transition regime theory needs to be applied in unlike-charged species collision rate calculations (Goree, 1992; Filippov, 1993; Khrapak et al., 2005; Gatti & Kortshagen, 2008; Gopalakrishnan & Hogan, 2012). The transition regime requires a much more detailed Natanson (1960) proposed a transition regime theory for ion-ion calculation approach. recombination, which was implemented by Hoppel & Frick (1986) to modify Fuchs's limiting sphere theory (Fuchs, 1963) towards more accurate calculations of recombination rates for small charged particle and ions (see also Marquard (2007) for an extended description of the limiting sphere theory and Stommel & Riebel (2007) for a detailed description of Hoppel & Frick's (1986) modifications). Ultimately, Hoppel & Frick's (1986) calculation approach was utilized in Wiedensohler developing the commonly-employed steady-state charge (Wiedensohler, 1988) for nanoparticles. However, while often overlooked, Hoppel & Frick's (1986) calculations require constants tuned specifically for air at ambient temperature and pressure. There are a variety of aerosol and plasma systems that do not operate at these conditions and where recombination rates need to be known. In particular, in non-thermal plasma synthesis reactors, semiconductor nanocrystals (e.g. Si nanocrystals) can be formed from the decomposition of hydride and chloride gases in argon or helium gas (Mangolini et al., 2005; Mariotti & Sankaran, 2010; Kortshagen et al., 2016; Lanham et al., 2021; Sawyer & Hart, 2021). While such reactors are typically near room temperature, they can be operated at a variety of pressures (from < 0.01 bar to atmospheric pressure). The nucleating nanocrystals interact with

electrons and argon or helium ions (positively charged), and the charge distribution of growing nanocrystals, beginning at the cluster stage, hinges upon the collision rate of negatively charged nanoclusters and positive gas ions, as cluster-electron collision rates are high and tend to bias charge distributions negative (Sawyer & Hart, 2021). An understanding of charging in these systems is important towards understanding and optimizing the synthesis process; if all clusters are negatively charged, then growth by cluster-cluster collisions is mitigated, while the proposed existence of neutral and positively charged clusters would permit coagulational growth to occur (Ravi & Girshick, 2009; Mamunuru *et al.*, 2017; Girshick, 2019; Santos *et al.*, 2019).

A more general collision rate theory for oppositely charged nanoparticles and ions, applicable for variable gas conditions, temperatures, and pressures was recently proposed by Gopalakrishnan and colleagues (Chahl & Gopalakrishnan, 2019; Li *et al.*, 2020; Li & Gopalakrishnan, 2020; Suresh *et al.*, 2021). Based on mean first passage time calculations with Langevin dynamics, implementation of the resulting rate equations yields good agreement with particle charge distributions measured in a variety of aerosol and plasma systems (Li, et al., 2020; Li & Gopalakrishnan, 2020; Husmann *et al.*, 2021; Suresh, et al., 2021). However, in analyzing nanocluster-ion recombination, the Langevin dynamics approach becomes computationally difficult to apply as the diffusive Knudsen number is high for nanocluster-ion encounters and the computational cost of Langevin dynamics simulations increases with the square of the diffusive Knudsen number (Gopalakrishnan & Hogan, 2011). Nanocluster-ion recombination at atmospheric pressure and reduced pressures is particularly difficult to examine through this approach.

There therefore remains a void in calculation procedures for the collision rate between unlike-charged nanoclusters and ions for arbitrary gas thermodynamic conditions and ion

properties. Recently, utilizing an implementation of flux-matching theory developed by Filippov (1993), we developed a combined continuum-molecular dynamics (C-MD) approach towards the calculation of recombination rates (Tamadate et al., 2020a; Tamadate et al., 2020b). In this approach all-atom models of the recombining species are considered, as is neutral background gas effects on motion. When the two species under consideration are a critical distance away from one another (the limiting sphere distance (Wright, 1960)), continuum modeling is employed to calculate the rate that one species migrates towards the other, and within this critical distance, molecular dynamics (MD) simulations are employed to determine if the encounter results in collision or not. The approach can be applied to nearly any type of species, provided accurate potential interactions are available, and can be applied across a wide temperature and pressure range. Herein, we adapt this approach to examine the recombination of Si nanocluster anions of the form Si_n^z where n = 47,91,266, & 494, z = -1, & -2 and Ar^+ at 300 K and pressures from $10^{3.5}-10^6$ Pa. In performing calculation for Si_n^z nanoclusters, we make use of manybody potentials (Stillinger & Weber, 1985), which are computationally more expensive than pairwise potentials. We develop a coarse-grained approach to improve computational efficiency when incorporating such potentials into the C-MD framework. The resulting collision rate coefficients are compared to Fuchs's (1963) limiting sphere theory as well as the more recent Langevin dynamics-based equations of Chahl & Gopalakrishnan (2019). Collision rate coefficients are then implemented in bipolar charge distribution model for clusters in a plasma, interacting with Ar⁺ and e⁻.

2. CALCULATION METHODS

The C-MD framework is described in detail in recent our studies of ion-ion recombination (Tamadate, et al., 2020b) and ion-macromolecular ion collisions (Tamadate, et al., 2020a). However, given the sparse use of this approach to date, we first briefly reintroduce the C-MD method in section 2a. Subsequently, the molecular dynamics simulation applied in C-MD are described in section 2b. Because the potential that is often utilized to described silicon nanoclusters (i.e. Si-Si bonds) in MD simulations includes many-body interactions (Stillinger & Weber, 1985), it is computationally more expensive than the potentials utilized in the previous C-MD calculations (Tamadate, et al., 2020a; Tamadate, et al., 2020b). Section 2b also provides a description of a method to utilize many-body potentials as the Ar⁺ ion approaches the Si_n^z nanoclusters, but with coarse-grained calculations at longer distances. In section 2c, we describe calculations to determine the charge distribution of of Si_n^z nanoclusters in a non-thermal plasma, where they are exposed to Ar^+ ions and free electrons.

a. C-MD Collision Rate Coefficient

Filippov (1993) showed that Fuchs' (1963) flux matching theory could be generalized to provide equations describing the collision rate coefficient (β_{ij} , describing collisions between type "i" and type "j" entities, with SI units of m³s⁻¹) between two species in an aerosol (i.e. surrounded by gas molecules). The result of his analysis is:

$$\beta_{ij} = \frac{4\pi(D_{+} + D_{-})\delta\Psi_{\delta}}{\left(1 - \exp(-\Psi_{\delta})\right)} \left(1 + \left(\frac{\pi}{2}\right)^{1/2} \frac{(2 - p_{\delta})}{p_{\delta}} K n_{\delta} \frac{\Psi_{\delta}}{(\exp(\Psi_{\delta}) - 1)}\right)^{-1}$$
(1a)

$$\Psi_{\delta} = -\frac{z_{+}z_{-}e^{2}}{4\pi\varepsilon_{0}k_{\mathrm{b}}T\delta} \tag{1b}$$

$$Kn_{\delta} = \left(\frac{m_{\text{red}}}{k_{\text{b}}T}\right)^{1/2} \frac{(D_{+} + D_{-})}{\delta} \tag{1c}$$

In equations (1a-1c), the subscripts "+" and "-" refer to Ar^+ and Si_n^z for the present study, D is the diffusion coefficient of the species in question, z is the number of charges (z_+) is always +1and z_{-} is -1 or -2), e is elementary charge, ε_{0} is vacuum permittivity, k_{b} is Boltzmann constant, T is temperature, and $m_{\rm red}$ is the Ar⁺ -Si^z_n reduced mass. The diffusion coefficients at atmospheric pressure (101325 Pa) and 300 K are summarized in table 1 for Si_n^z nanoclusters, while the diffusion coefficient of Ar⁺ in Ar gas under these conditions is $D_+ = 0.04$ cm² s⁻¹, known from measurement (Madson & Oskam, 1967). The diffusion coefficient is inversely proportional to the pressure, and hence easily changed for calculations at reduced and elevated pressures. The diffusion coefficients of Si_n^z used were calculated directly from MD simulations; specifically we determine mean square displacement (MSD) of the center of mass of each Si_n^z nanocluster tested in Ar, subject to all-atom potentials as described in section 2c, with further details in the supporting information, including comparison to diffusion coefficients from velocity autocorrelation functions. The MSD-based Si_n^z diffusion coefficients were also utilized to decide the collision distance of each size of Si_n^z cluster with Ar^+ . The collision cross section, Ω , can be calculated from the diffusion coefficient via the Mason-Schamp equation (Mason & McDaniel, 1988; Larriba-Andaluz & Prell, 2020; Larriba-Andaluz & Carbone, 2021), and the collision cross section can be used to approximate the collision distance L by assuming Si_n^z is a spherical, diffuse scatterer, leading to $\Omega = 1.36\pi L^2$. Table 1 also shows the calculated collision distance for each silicon nanocluster in argon.

With diffusion coefficients calculable, this leaves two unknown parameters in equations (1a-c); δ , the limiting sphere radius, yielding the limiting sphere diffusive Knudsen number Kn_{δ} , and p_{δ} , the probability that two of the entities approaching one another from a distance δ will collide with one another, rather than move away from one another. Importantly, Filippov (1993)

notes that provided δ is sufficiently large such that the continuum mass transfer approximation applies beyond δ and p_{δ} is calculated with a correct approach, equation (1a-c) will yield the collision rate for all possible gas temperatures and pressures (note Fuchs (1963) utilized free molecular motion for p_{δ} , which is not correct for the present case of unlike charged entities near atmospheric pressure). Therefore, in C-MD, an important aspect is tuning δ and calculating β_{ij} for different δ values in order to ensure β_{ij} converges in the large δ limit. Figure 1(a) depicts the C-MD simulation environment used in p_{δ} calculation, with an assumed δ value. As shown in blue arrows, the Ar⁺ ion enters the limiting sphere with the Si^z_n ion at the center of the domain. The motion of both species is monitored via MD simulations (figure 1b) until either collision occurs (i.e. when their centers of mass are within L of one another) or their separation distance exceeds δ . MD simulations, described in the next section, are repeated for multiple instances until 100 collision events are observed (yielding p_{δ} to within 10% of its determined value); p_{δ} is equal to 100 divided by the total number of simulations required to yield 100 collision events.

For the present study, the tuned values of δ shown in table S1 and table S2 of the supporting information were applied. As noted in the prior paragraph δ must be large enough to apply in the large δ limit, however, the smallest δ possible is desirable to minimize computational time. To decide δ , we performed β_{ij} calculation with only smallest cluster Si_{47}^z , varying δ over the pressure range $10^{3.5}-10^6$ Pa for both z=-1 and z=-2. In Fuchs's theory, δ is commonly calculated from the equation proposed by Wright (1960), which is based on the physical size (capture radius) of the colliding species and not a function of the magnitude of long range potential interactions. We first calculated δ as the traditional value (δ_{Fuchs}) for the optimization of δ . Figure 2 shows results for z=-1 with different pressures and the x-axis is δ normalized by δ_{Fuchs} from Wright's theory at 300 K. The large δ limit can be found for each

pressure from these results, and for subsequent calculations we employed as small as safely possible a δ/δ_{Fuchs} value from these curves, for all clusters (utilizing the same δ/δ_{Fuchs} for all nanoclusters at a given pressure, as obtained for optimization the Si_{47}^z with z=-1 and z=-2, with δ_{Fuchs} recalculated for each nanocluster). We remark that because Si_{47}^z is the smallest nanocluster examined, from the strength of the potential influence acting on the nanocluster, deviations in the required δ from δ_{Fuchs} should be the largest, hence extrapolation of the δ/δ_{Fuchs} value inferred from sensitivity analysis with Si_{47}^z is reasonable. However, to mitigate any additional cluster size effect on calculations, we applied a slightly larger limiting sphere than the smallest value than was found acceptable for converged calculations (i.e. $\delta/\delta_{Fuchs}=0.3$ is found acceptable in many instances, but we nonetheless employed $\delta/\delta_{Fuchs}=1.0$). MD simulations to evaluate δ/δ_{Fuchs} were performed considering neutral gas, as noted subsequently.

In addition to p_{δ} calculation, MD simulations permit observation of the behavior of Si_n^z nanoclusters after collision to examine translational energy transfer from the impinging Ar^+ ion to the nanocluster. MD simulations were continued for 10 ps after the collision event, with electrical interactions between the Si_n^z and Ar no longer considered, as the Ar^+ was assumed to have transferred its charge to the nanocluster. The Ar^+ ion loses kinetic energy to the Si_n^z nanocluster during collision. From the initial velocity v_i at the collision distance and reflection velocity v_o of Ar^+ determined after the collision, the lost kinetic energy of Ar^+ , ΔK_E for each Argon ion is defined as:

$$\Delta K_{\rm E} = \frac{m_{+}}{2} (v_{\rm o}^2 - v_{\rm i}^2) \tag{2}$$

While some energy is transferred to neutral gas during approach and impingement, $\Delta K_{\rm E}$ calculation and comparison to the internal energy of the nanocluster enables estimation of the contribution of translational energy-to-thermal energy transfer on nanocluster heating. This is

important because in non-thermal plasma synthesis systems, crystalline nanomaterials are typically produced; this requires heating of growing nanocrystals, yet the mechanism of heating in such systems in not yet completely clear (Mangolini & Kortshagen, 2009; Kramer *et al.*, 2014; Uner & Thimsen, 2018).

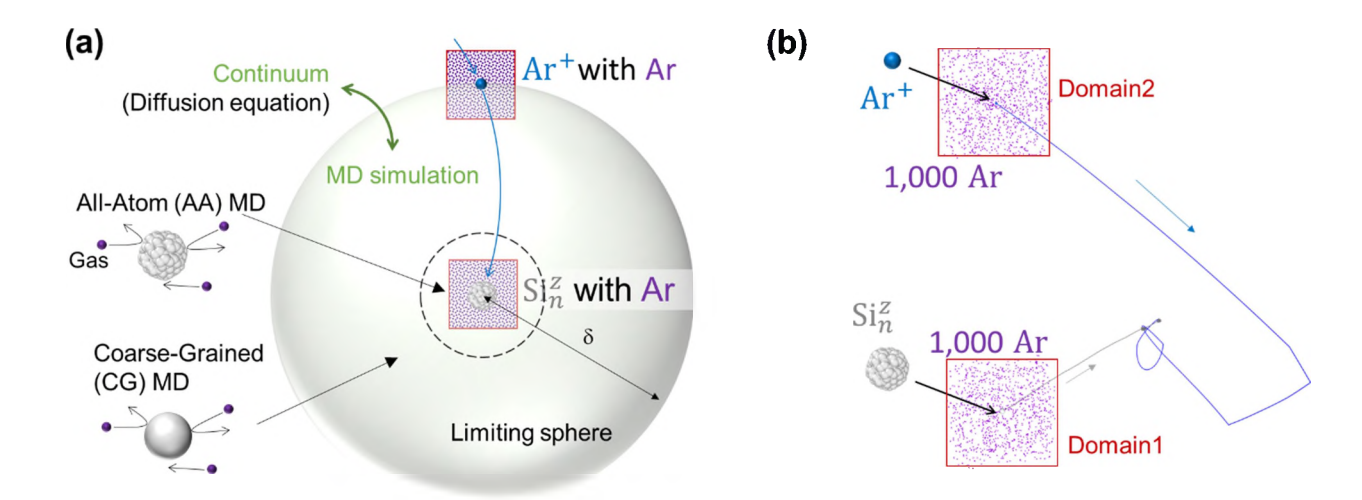


Figure 1. A depiction of the C-MD spherical simulation domain. Beyond the limiting sphere, continuum mass transfer describes ion and nanocluster migration, while molecular dynamics simulation is employed within the limiting sphere. The dashed spherical region denotes the cutoff between the coarse-grained region where the Si_n^z nanocluster is approximated as a bulk sphere and the region where all-atom motion is monitored (a). A depiction of a Si_n^z nanocluster and Ar^+ ion trajectories including their assigned neutral gas atoms, which only interact with their assigned charged species (b).

Table 1. A summary of the diffusion coefficients and collision distances of Si_n^z nanoclusters, with n noted.

Number of Atoms	47	91	266	494
Diffusion coefficient at 1 atm, D_0 [cm ² /s]	1.6 x 10 ⁻²	1.1 x 10 ⁻²	6.5 x 10 ⁻³	5.3 x 10 ⁻³
Collision distance, L [Å]	8.4	11.7	13.2	14.6

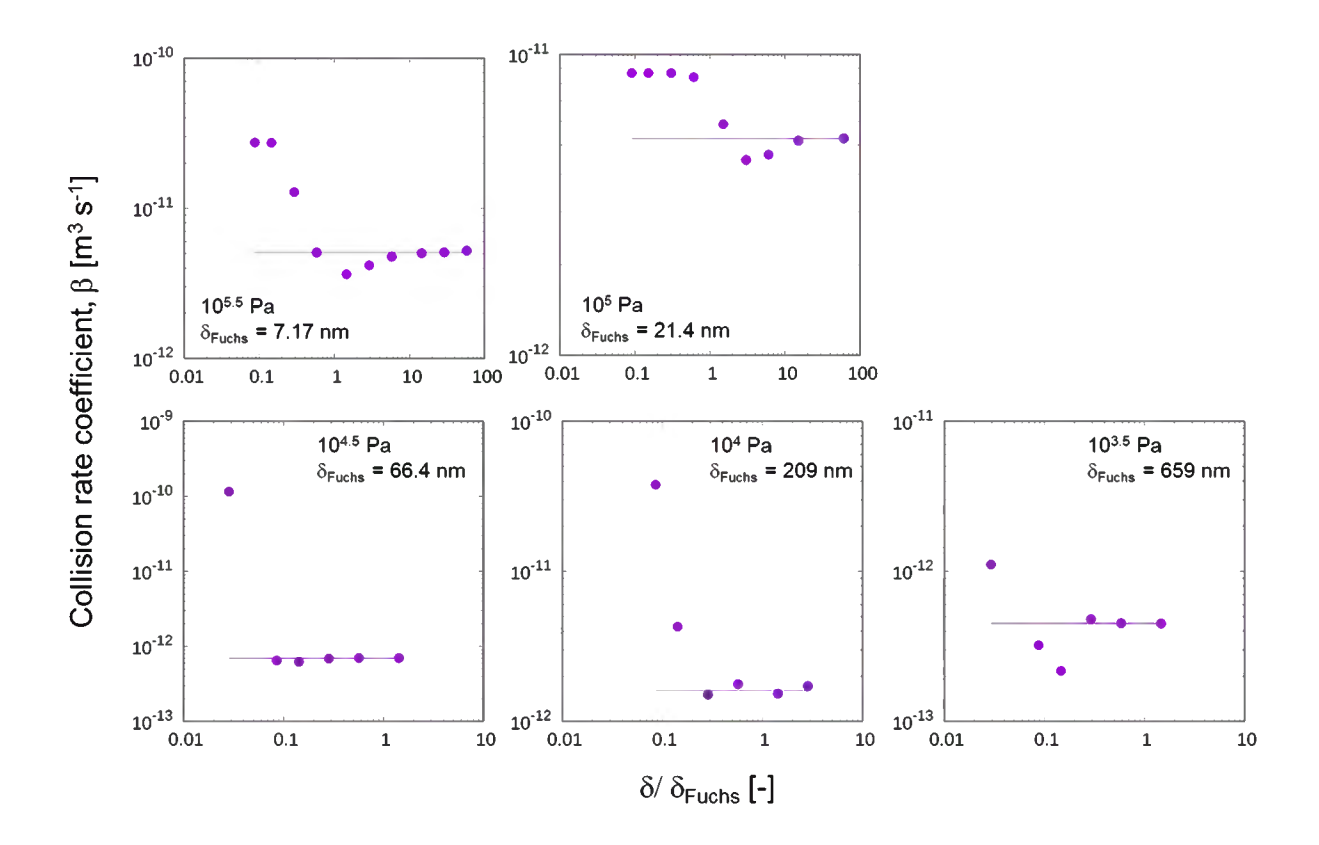


Figure 2. Sensitivity analysis of the collision rate coefficient using the Si_{47}^{-1} nanoclusters wherein the C-MD collision rate (recombination rate) coefficient is calculated as a function of δ/δ_{Fuchs} .

b. Molecular Dynamics Simulations

In C-MD simulations, the MD domain is a sphere of radius δ which is constantly recentered on the Si_n^z center-of-mass as the simulation proceeds. To account for the influence of neutral gas on Si_n^z and Ar^+ motion, both the nanocluster and ion are surrounded by cubical domains containing 10^3 Ar atoms each, with the domain side length determined by the simulation pressure and temperature. These Ar atoms only interact with their assigned charged species and not with one another, mimicking free molecular momentum transfer but transition regime mass transfer for both Si_n^z and Ar^+ (Tamadate, et al., 2020b). Periodic boundary conditions are applied on the cubic domain walls, and each gas atom is initiated with a random directional vector and a speed sampled from the Maxwell-Boltzmann speed distribution. The

periodic boundary conditions result in a small amount of translational energy increase as simulation evolve (because the Si_n^z and Ar^+ move at higher velocities, due to attractive Coulomb potentials). However, we find this does not adversely impact simulation results with 10^3 gas atoms employed.

To initialize simulations, the Ar⁺ ion is placed on the limiting sphere boundary (as noted in the prior section), and initiated considering both its thermal velocity and the velocity based its mobility and the electrostatic force. Specifically, the thermal velocity is considered in three directions (v_x, v_y, v_z) with each component sampled from a Maxwell-Boltzmann distribution via a Mersenne Twister pseudorandom number generator. Additionally an electrophoretic velocity is added toward the Si_n^z nanocluster direction (y-direction), as calculated the product of the ion mobility and the electrostatic force at the outer sphere radius. Further details on velocity initialization part are described in Tamadate et al (2020b). A spherical Si nanocluster is also cut from a bulk Si crystal and the cluster, now with a prescribed number of atoms. The Si_n^z nanocluster is thermally stabilized via NVT simulations at 300 K with a Nose-Hoover thermostat, in the absence of background gas for 200 ns. Following removal of the center-ofmass translational velocity, the Si_n^z nanocluster is then randomly rotated and placed in the domain center. The 200 ns initial calculation is only performed in the beginning of the simulation (N = 1), and for the later simulations (later collision trials), 0.1 ns of additional calculation is applied to yield a different structure. Gas atoms are then placed around the Si_n^z nanocluster and Ar⁺ ion.

Only a single cation and nanocluster anion are simulated; hence our calculations apply in the "dilute" limit wherein the probability of multiple cations or mulitple anions being present during cation-nanocluster anion close approach is negligibly low. With simulations initiated and gas atom domains assigned, collision simulation is performed without thermostatting, using a velocity-Verlet algorithm to solve the equations of motion with a time step of 1.0 fs. Each "run" results either in collision, i.e. the two species are closer than the previously described collision distance, or non-collision, where the Ar⁺ leaves the limiting sphere. Minimization of computation time is important in calculations as we target 10^2 collision events for each scenario examined, and this can require up to 10^7 distinct simulations. Towards increased computational efficiency, the domain is further divided into two subdomains. In the inner domain, which is a spherical region of radius 10 nm (which is always less than δ), all-atom potential interactions are considered. Both Si/Ar and Ar/Ar potential interactions are described with the Lennard-Jones 6-12 potential and a Coulombic potential. Specifically, the magnitude of the interaction (U_{ij}) between atoms i and j with a center-of-mass separation distance of r_{ij} is given in following equation:

$$U_{ij} = 4\epsilon_{ij} \left[\left(\frac{\sigma_{ij}}{r_{ij}} \right)^{12} - \left(\frac{\sigma_{ij}}{r_{ij}} \right)^{6} \right] + \frac{z_{i}z_{j}}{4\pi\epsilon_{0}r_{ij}}$$
(2)

where σ_{ij} and ϵ_0 are the potential parameters determining the Lennard-Jones potential shape. We apply $(\sigma_{ij}, \epsilon_{ij}) = (3.903, 0.2152)$ and (3.401, 0.2339), with σ_{ij} in Angstrom and ϵ_{ij} in kcal mol⁻¹ (conventionally employed in molecular simulations) for Si/Ar and Ar/Ar interactions, respectively. The parameters z_i and z_j are the partial charges of atoms i and j, respectively. +1 was used for the Ar⁺ and for the Si atoms, the total charges divided by the number of atoms composed the cluster was applied, e.g., -1/47 = -0.0213 was placed on each Si in Si⁻₄₇ cluster. The bonding of Si-Si is more complex. It is a covalent bond where the strength of the bond depends upon the positions of multiple Si atoms. To reflect this, we used the many-body Stillinger-Weber (SW) potential (Stillinger & Weber, 1985), expressed as:

$$U = \sum_{i} \sum_{i>j} \varphi_2(r_{ij}) + \sum_{i} \sum_{j\neq i} \sum_{i>j} \varphi_3(r_{ij}, r_{ik}, \theta_{ijk})$$
(3a)

$$\varphi_2(r_{ij}) = A\epsilon \left[B \left(\frac{\sigma}{r_{ij}} \right)^q - \left(\frac{\sigma}{r_{ij}} \right)^p \right] exp \left(\frac{\sigma}{r_{ij} - a\sigma} \right)$$
 (3b)

$$\varphi_3(r_{ij}, r_{ik}, \theta_{ijk}) = \lambda \epsilon \left[\cos\theta_{ijk} - \cos\theta_0\right]^2 \exp\left(\frac{\gamma \sigma}{r_{ij} - a\sigma}\right) \exp\left(\frac{\gamma \sigma}{r_{ik} - a\sigma}\right)$$
(3c)

The second term of equation (3a) represents two-body interactions and the third term accounts for three-body interactions. The parameters are given as A=7.49556277, B=0.6022245584, $\varepsilon=2.1683$ eV, $\sigma=2.0951$ Å, q=1, p=4, $\lambda=21.0$, $\gamma=1.2$, $\alpha=1.8$, $\theta_0=\frac{1}{3}$. As this potential require three computational loops for indexes i,j and k, the computational cost is much higher than that of Lennard-Jones potentials and other pair-wise potentials.

At far separation distance for the Si_n^z nanocluster and Ar^+ ion, all-atom modeling with the SW potential is both impractical and unnecessary. We therefore apply a coarse-grained model for Si_n^z nanoclusters when the Si_n^z - Ar^+ in the outer MD domain, beyond 10 nm separation distance. In this region, the Si_n^z nanocluster is treated as a sphere and only the Coulomb potential between the Si_n^z nanocluster and Ar^+ ion is considered. At 10 nm separation distance, the Si/Ar potential interaction is negligible in comparison to thermal energy. With the coarse-grained model the interaction of the Si_n^z nanocluster with neutral Ar gas is calculated as shifted Lennard Jones potential:

$$U_{ij} = 4\epsilon_{ij} \left[\left(\frac{\sigma_{ij}}{r_{ij} - r_0} \right)^{12} - \left(\frac{\sigma_{ij}}{r_{ij} - r_0} \right)^{6} \right]$$

$$\tag{4}$$

Si/Ar parameters are used as a parameter set, $\sigma_{ij} = 3.903 \,\text{Å}$ and $\epsilon_{ij} = 0.2152 \,\text{kcal mol}^{-1}$, and $r_0 = L - \sigma_{ij}$, the collision radius from diffusion coefficient calculations. If collision-rates were our only concern, the coarse-grained model could likely be used for the entire calculation. However, as noted in section "2a: C-MD Collision Rate Coefficient," our interests are also in

examining ion translation energy to thermal energy conversion upon collision. Heat transfer in collisions MD simulations is strongly dependent on the potential interactions both between and within the colliding bodies (Sipkens & Daun, 2018), hence we aim to utilize as accurate a model of Si-Si bonding as possible during the collision. Furthermore, to our knowledge, a distance-dependent coarse-grained approach has not been utilized in simulations relevant to aerosol transport phenomena previously and in applying it here we seek to establish this as a tractable calculation route for aerosol transport and collisional phenomena.

c. Charge Distribution Modeling

Ultimately, collision rate calculations need to be incorporated into population balance models or other approaches to determine charge distributions (Wiedensohler, 1988; Matsoukas & Russell, 1995; Deser & Kuhne, 2021). The present study is specifically motivated by the need to better understand nanocluster charge distributions in non-thermal plasma synthesis systems (Sawyer & Hart, 2021), where the positive ions are Ar^+ and the negative charge carriers are free electrons (e⁻). Though there is some evidence that free electrons may play a role in particle charging in N_2 in electrostatic precipitators (Bürger & Riebel, 2020), the disparity in mobility and masses between Ar^+ and e⁻ leads to unique nanocluster and particle charge distributions in non-thermal plasmas, further making important accurate calculation of the Si_n^z - Ar^+ collision rate for negatively charged nanoclusters. We examine steady-state charge distributions for Si_n nanoclusters in a 300 K plasma where the electron temperature is 2 eV, and n spans the range used in C-MD calculations (n = 47 - 494). The time rate of change in the number concentration of nanoclusters (N_z) of charge state z is given by the population balance equation:

$$\frac{dN_z}{dt} = \beta_{z-1}^+ N_{Ar^+} N_{z-1} - \beta_z^+ N_{Ar^+} N_z + \beta_{z+1}^- N_{e^-} N_{z+1} - \beta_z^- N_{e^-} N_z$$
 (5)

where the subscripts Ar+ and e- denote the argon ion and free electron densities, respectively and β_z^+ denotes the collision rate coefficient for charge state z nanoclusters with positive ions (with "-" applied for electrons). We assume $N_{\rm Ar^+}=N_{\rm e^-}$ (electroneutrality is satisfied in the plasma, with the particle concentration significantly smaller than the ion density) and hence the ion and electron densities cancel out completely in the steady-state solution of equation (5). Because of their high kinetic energies, leading to large persistence distances, the Si_n and electron collision rate coefficient at all studied pressures can be describe by traditional orbital motionlimited theory, (Mott-Smith & Langmuir, 1926; Allen, 1992) also referred to as the free molecular approach. This rate expression is hence employed for all $\mathrm{Si}_n - \mathrm{e}^-$ collisions for all possible charge states. To compare results to alternatives, here we employ three distinct approaches for the Si_n^z -Ar⁺ collision rate coefficient: (1) results from C-MD calculations, (2) Fuchs (1963) original approach, unmodified, and (3) the theory of Chahl & Gopalakrishnan (2019). Equation (5) is solved for the range z = -6, -5, ..., 0, ... + 6, as $t \to \infty$ using a 4th order Runge-Kutta scheme. In case (1), with C-MD simulations, results are only available for the z = -1 & -2 nanoclusters, and for all other charge states with Ar⁺ ions we employ the Chahl & Gopalakrishnan (2019) rate coefficient. We remark that because of their nanometer scale size, the z = -1 & -2 are likely to be the most important (i.e. possibly most abundant) charge states for nanoclusters in a plasma environment. For both Fuchs (1963) and Chahl & Gopalakrishnan (2019) calculations, Ar^+ ion and Si_n^z diffusion coefficients are identical to those input into C-MD calculations for the pressure in question and collision distance was that inferred from mean square displacement calculations.

3. RESULTS AND DISCUSSION

a. C-MD Calculation Results

While we do not carry out calculation validation explicitly in the current work, we remark that in our first study utilizing the C-MD approach (Tamadate, et al., 2020b) we examine the validity of calculations in detail, first showing that in the absence of neutral in MD calculations (leading completing free molecular or ballistic trajectories for the charged species) calculations recover the collision rate coefficients predicted by Fuchs (1963). In the high pressure and low pressure limits, C-MD calculated collision rate coefficients recover values in excellent agreement with continuum and free molecular mass transfer models, respectively. We also demonstrated that at atmospheric pressure, ion-ion recombination rate coefficients in helium gas calculated via the C-MD method agree well with measurements by Lee & Johnsen (1989). Furthermore, C-MD collision rate coefficients were previously compared to values inferred experimentally for macromolecular ion neutralization in N2, with reasonable agreement between experiments and calculations (Tamadate, et al., 2020a). Combining these results, we believe that C-MD calculations are sufficiently developed that their results can now be employed to specifically examine collision rate phenomena in aerosol systems, such as the present examination of $Si_n^z - Ar^+$ collisions, even if direct experimental measurement of this rate has not yet been accomplished. That stated, C-MD calculations are certainly affected by the choice of potentials as well as input values for the properties of the colliding species and neutral gas, hence the subsequently presented specifically apply for the models of Si_n^z and Ar^+ utilized.

Figures 3 and 4 display plots of the collision rate coefficient for the four examined Si_n^z nanocluster sizes as a function of gas pressure at 300 K, for z = -1 and z = -2, respectively. In addition to displaying C-MD results, these figures also plot the free molecular limiting

expression (Allen, 1992), and the continuum limit expression original proposed by Langevin (1903), which is also calculable via Fuchs's enhancement factor equation considering attractive Coulomb potentials (Fuchs, 1964). We also plot Fuchs's (1963) transition regime theory and Chahl & Gopalakrishnan's (2019) theory. For both charge states, we generally find that C-MD calculations are intermediate to not only the free molecular and continuum limiting expresssions, but also the Fuchs (1963) and Chahl & Gopalakrishnan (2019) calculated rate coefficients. C-MD collision rate coefficients are higher than Fuchs (1963) predictions in nearly all circumstances, but lower than Chahl & Gopalakrishnan (2019) predictions. coefficients than Fuchs (1963) predictions are anticipated as a known issue with the original incarnation of limiting sphere theory is the underprediction of collision rate coefficients for unlike charged, nanometer scale species. The disagreement with Chahl & Gopalakrishnan (2019) predictions is consistent with the disagreement with observed in examining this theory for macromolecular ion neutralization (Tamadate, et al., 2020a); the two distinct calculation approaches fall within an order of magnitude of one another, but the Chahl & Gopalakrishnan (2019) expression tracks more closely the continuum limit expression at high pressures, particularly for the z = -2 charge state. Overall, calculations highlight that even at low pressures (with 10^{3.5} Pa the minimum studied here), the collision rate coefficient between unlike charged, nanometer scale species cannot be calculated by free molecular rate expressions, and with none of the existing theories which permit a priori rate calculation agreeing with C-MD calculations, accurate recombination rate calculations at present require a detailed approach for calculation, such as the C-MD method. As discussed in Tamadate et al., (2020b), the Hoppel & Frick (1986) calculation approach could be fit to C-MD calculation results, but does require as an input a "trapping distance" which is typically determined from knowledge of the recombination rate coefficient itself.

At the same time, as many aerosol and microplasma systems operate near atmospheric pressure, i.e. near 10⁵ Pa (Chen *et al.*, 2018; Gallingani *et al.*, 2020; Sharma *et al.*, 2020). At this pressure, C-MD inferred rate coefficients for singly charged nanoclusters agree well with those from Fuchs (1963), particularly considering C-MD recombination rate coefficients have a Poisson-statistic uncertainty of 10% (which can be reduced by increasing the number of collision events in rate determination). While the Chahl & Gopalakrishnan (2019) expression deviates from the other two at 10⁵ Pa, for the doubly charged nanoclusters, the recombination rate for all three approaches aligns well with the Langevin continuum limit expression near atmospheric pressure.

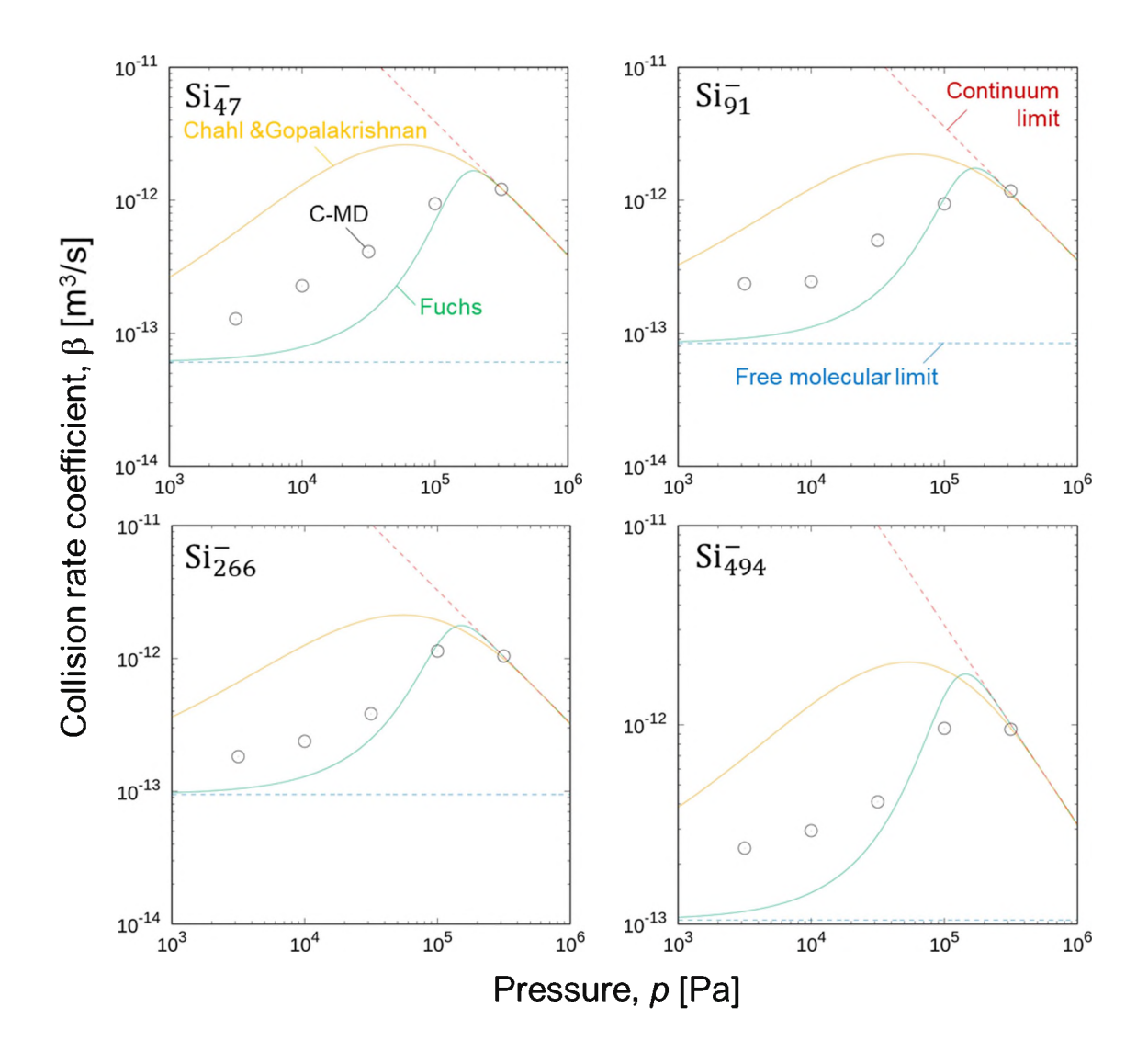


Figure 3. Si_n^z - Ar^+ collision rate coefficients calculated via the C-MD method (circles) as a function of Ar neutral gas pressure at 300 K, for z=-1, with n noted in each subfigure. The red and blue dashed lines represent the continuum and free molecular limits, respectively, the yellow curve is the Chahl & Gopalakrishnan (2019), expression prediction and the green curve is the predictions of Fuchs (1963).

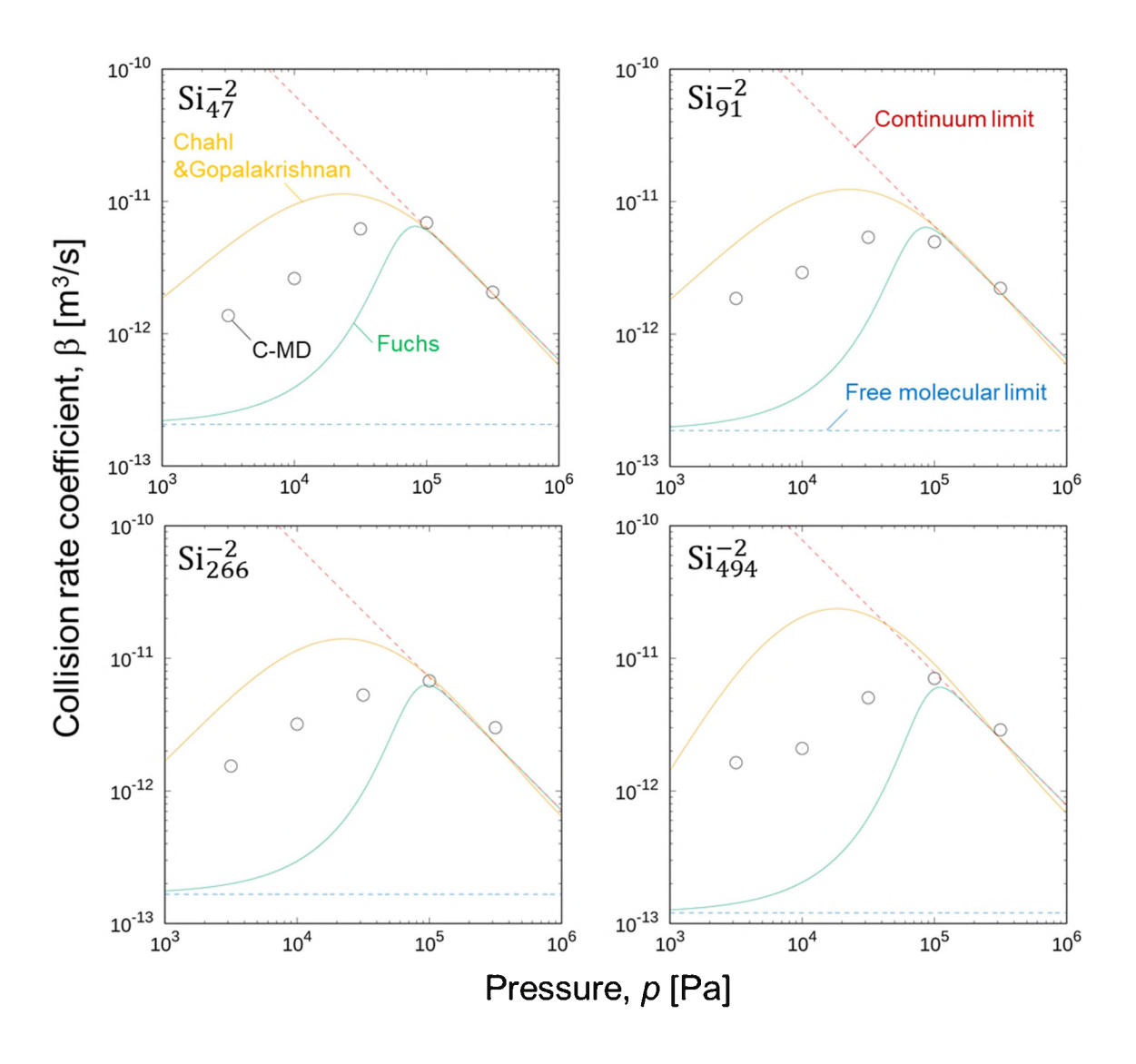


Figure 4. Si_n^z - Ar^+ collision rate coefficients calculated via the C-MD method (circles) as a function of Ar neutral gas pressure at 300 K, for z=-2, with n noted in each subfigure. The red and blue dashed lines represent the continuum and free molecular limits, respectively, the yellow curve is the Chahl & Gopalakrishnan (2019), expression prediction and the green curve is the predictions of Fuchs (1963).

Beyond the collision rate, of interest in non-thermal plasma systems is an understanding of collisional heat transfer between growing nanoclusters and their surroundings, primarily because they are room temperature or near room temperature systems with demonstrated ability to both produce crystalline nanomaterials (Kortshagen, 2016) and to evaporate materials (Uner & Thimsen, 2017; Uner & Thimsen, 2018; Uner *et al.*, 2019). A model of the heating of growing

nanocrystals in non-thermal plasma environments was developed by Mangolini & Kortshagen (2009) and included heating due $Ar^+ - e^-$ recombination at the surface of a growing nanocrystal as well as heat transfer from the nanocrystal to the surrounding neutral gas (Sipkens & Daun, 2018; Yang et al., 2022), and can be adapted to include addition terms, such as the latent heat release due to condensation and coagulation growth (Yang et al., 2019). One possible heating mechanism not considered in prior work is translational energy transfer to thermal energy transfer when a high velocity Ar^+ impinges upon a Si_n^z nanocluster surface. Figure 5a plots a histogram of the change in Ar⁺ kinetic energy for 10² collision events with a Si₄₇ nanocluster at 10⁵ Pa and 300 K. Because of the strong attractive Coulomb potential the Ar⁺ velocity at collision is well beyond the mean thermal speed of the neutral gas. Nonetheless, we observe that the change in translational energy for the Ar^+ is of order k_bT . Because this change in the translational energy is distributed over 47-500 Si atoms, the per atom energy gained in Si_n^z nanoclusters is less than k_bT near 300 K. Therefore, it does not appear that translational energyto-thermal energy transfer (in the Si_n^z nanocluster) is a significant heating mechanism in nonthermal plasma environments. To further demonstrate this, in figure 5b we plot $\Delta \overline{K_E}$, the mean change in Ar⁺ translational energy for 10⁵ and 10^{3.5} Pa, as a function of the number of atoms in the silicon nanocluster examined. Mean kinetic energy changes are significantly lower than the Si-Si bond energy and only modestly higher than k_bT . As the energy transferred to the nanocluster is distributed to a large number of atoms, the heat transfer remains small in all circumstances on a per-collision basis. At the same time, it is noteworthy that the mean kinetic energy change increases both for doubly charged nanoclusters over their singly charged counterparts as well as for smaller nanoclusters. Both of these observations are attributable to

the higher velocities of Ar⁺ at the moment of collision, which is brought about by the increased influences of the Coulomb potential for higher charge states and closer distances.

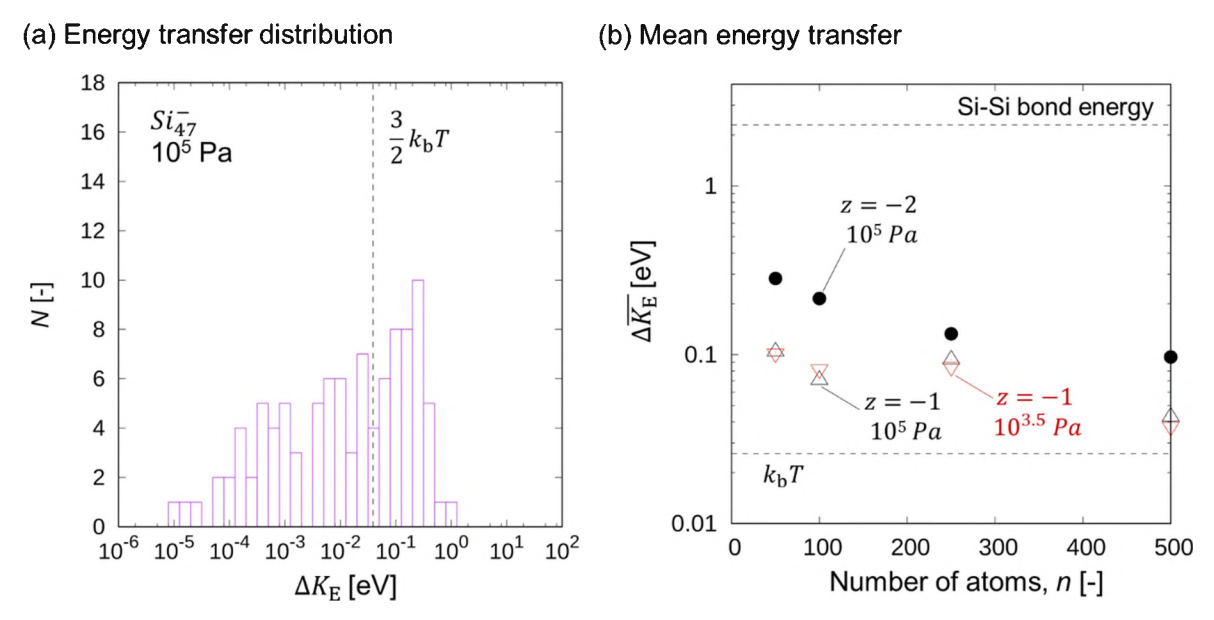


Figure 5. Histogram of $\Delta K_{\rm E}$, the change in Ar⁺ translational energy during collision with an Si₄₇ nanocluster at 10⁵ Pa and 300 K (a). The mean change Ar⁺ translational energy during collision in $\Delta \overline{K_{\rm E}}$ as a function of the number of atoms in the silicon nanocluster (b).

b. Silicon Nanocluster Charge Distributions

The steady-state solutions for the charge population balance equations (5) for Si_n nanoclusters in a non-thermal argon plasma with an electron temperature of 2 eV are shown in figures 6 and 7 for argon neutral pressures of 10^5 Pa and $10^{3.5}$ Pa, respectively. These results are also provided in tables 2 and 3. Solutions utilizing C-MD results for the singly and doubly charged recombination rate, as well as solely the Chahl & Gopalakrishnan (2019) equations and Fuchs's (1963) limiting sphere theory are provided. First examining calculations near atmospheric pressure, when examined on a logarithmic scale, the three calculation approaches appear to give similar results, i.e. all three calculation approaches yield charge fractions within an order of magnitude of one another for each examined charge state. However, as evidenced in

table 2, differences in charge distributions are evident, with Fuchs's (1963) limiting sphere theory yielding charge distributions most biased towards negative values, followed by C-MD based calculations, and the Chahl & Gopalakrishnan (2019) rate coefficients yielding the largest fraction of neutral particles under all conditions. This is expected, as Fuchs's (1963) limiting sphere theory yields the lowest recombination rate, C-MD calculations intermediate, and Chahl & Gopalakrishnan (2019) the highest, but highlights that even at atmospheric pressure, where predicted recombination rates are close to the continuum limit expressions, differences do exist between different theories. We do regard C-MD calculations as likely the most accurate of the three tested, as they are based upon all-atom models with fewer assumptions than the other approaches. Importantly, all three theories predict that at steady-state, the fraction of positively charged nanoclusters is extremely low, below 2×10^{-4} for all Si_n nanoclusters. This is consistent with the calculations of Chen & Hogan (2021) for larger silicon nanocrystals in a non-thermal plasma environment, and in total existing theories do not predict that a significant fraction of nanoclusters or nanoparticles would be positively charged in a plasma environment. However, a non-negligible fraction is expected to be neutral, with all theories predicting an increased neutral fraction with decreasing nanocluster size. Non-thermal plasma synthesis reactors typically operate under conditions with high precursor gas concentrations (Chen et al., 2020) and hence would have a high rate of nanocluster-nanocluster collisions in the absence of Coulombic repulsion. Therefore, C-MD calculations, along with other theories, suggest that neutral nanocluster collisional growth, both with other nanoclusters and with larger nanoparticles of any charge state is an important growth mechanism in non-thermal plasma systems, as proposed and examined by Girshick and colleagues (Ravi & Girshick, 2009; Agarwal & Girshick, 2012; Le Picard et al., 2016; Mamunuru, et al., 2017; Girshick, 2019).

At reduced pressure, qualitatively, charge distributions show the same trends as atmospheric pressure calculations, with Fuchs's (1963) rate coefficients yielding the most negatively biased charge distributions and Chahl & Goplakrishnan's (2019) calculations yielding the least negatively biased charge distributions. However, the differences between the distinct collision rate coefficient theories are much more pronounced at reduced pressure. The highlights the need for highly accurate collision rate calculation methods when examining aerosols of nonstandard pressure, temperature, and gas composition. Particularly striking are the distinctions in charge distributions between Fuchs's (1963) rate coefficients and the other two calculation methods. The large difference between Fuchs-based (1963) calculations and C-MD results at reduced pressure in comparison to atmospheric pressure, can perhaps explain why in atmospheric pressure systems limiting sphere theory forms is the standard approach to steadystate charge distribution calculations (Wiedensohler, 1988), while when limiting sphere theory was re-introduced to examine charge distributions for particles in reduced pressure plasmas (D'yachkov et al., 2007), it was immediately noted that limiting sphere predictions were not in agreement with other theories and with measurements (Gatti & Kortshagen, 2008).

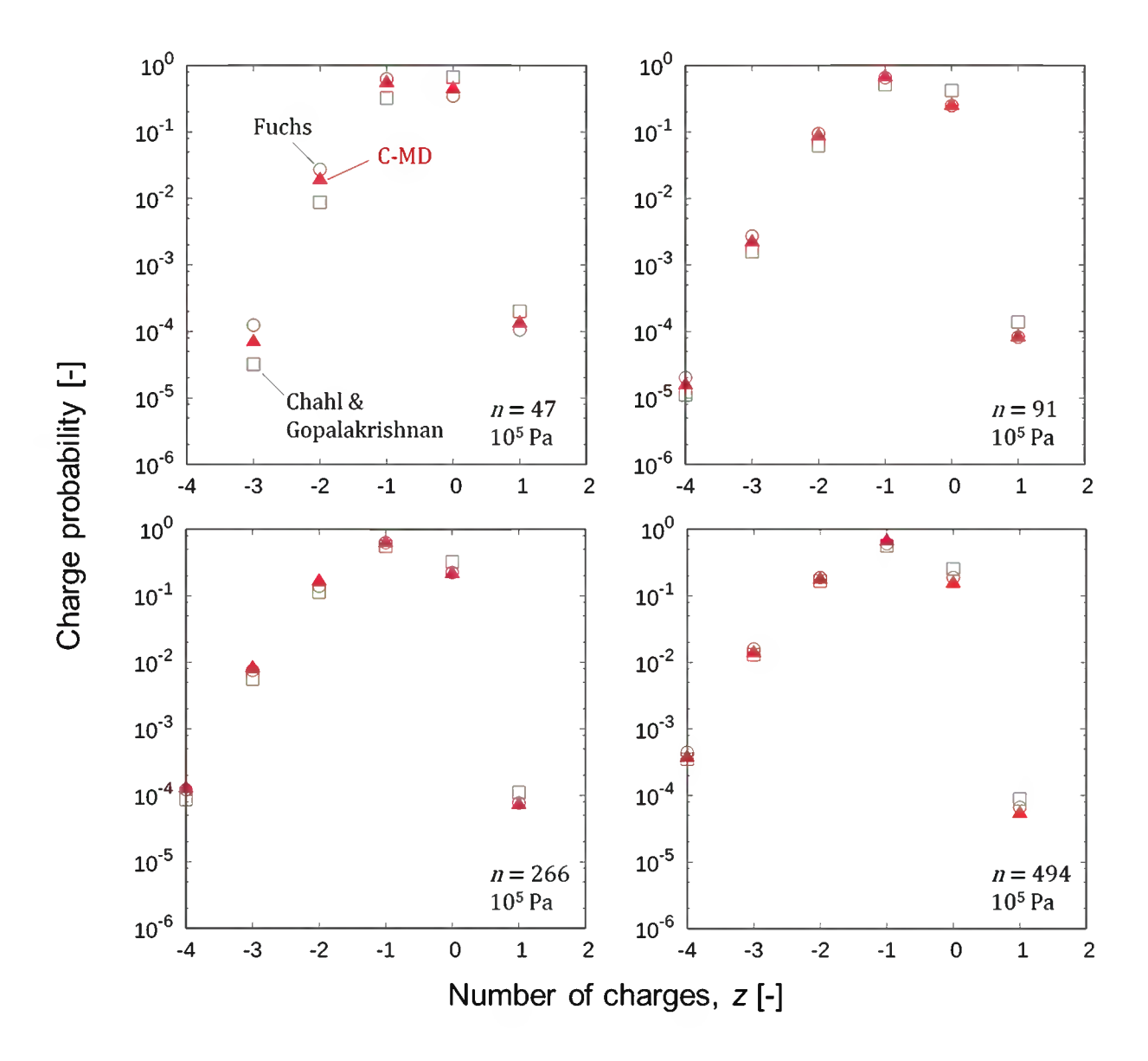


Figure 6. The steady-state charge distributions of Si_n nanoclusters in a non-thermal argon plasma at 10^5 Pa and 300 K, with an electron temperature of 2 eV. Circles: Rate coefficients from Fuchs (1963); Square: Rate coefficients from Chahl & Gopalakrishnan (2019), and triangle: C-MD recombination rate coefficients.

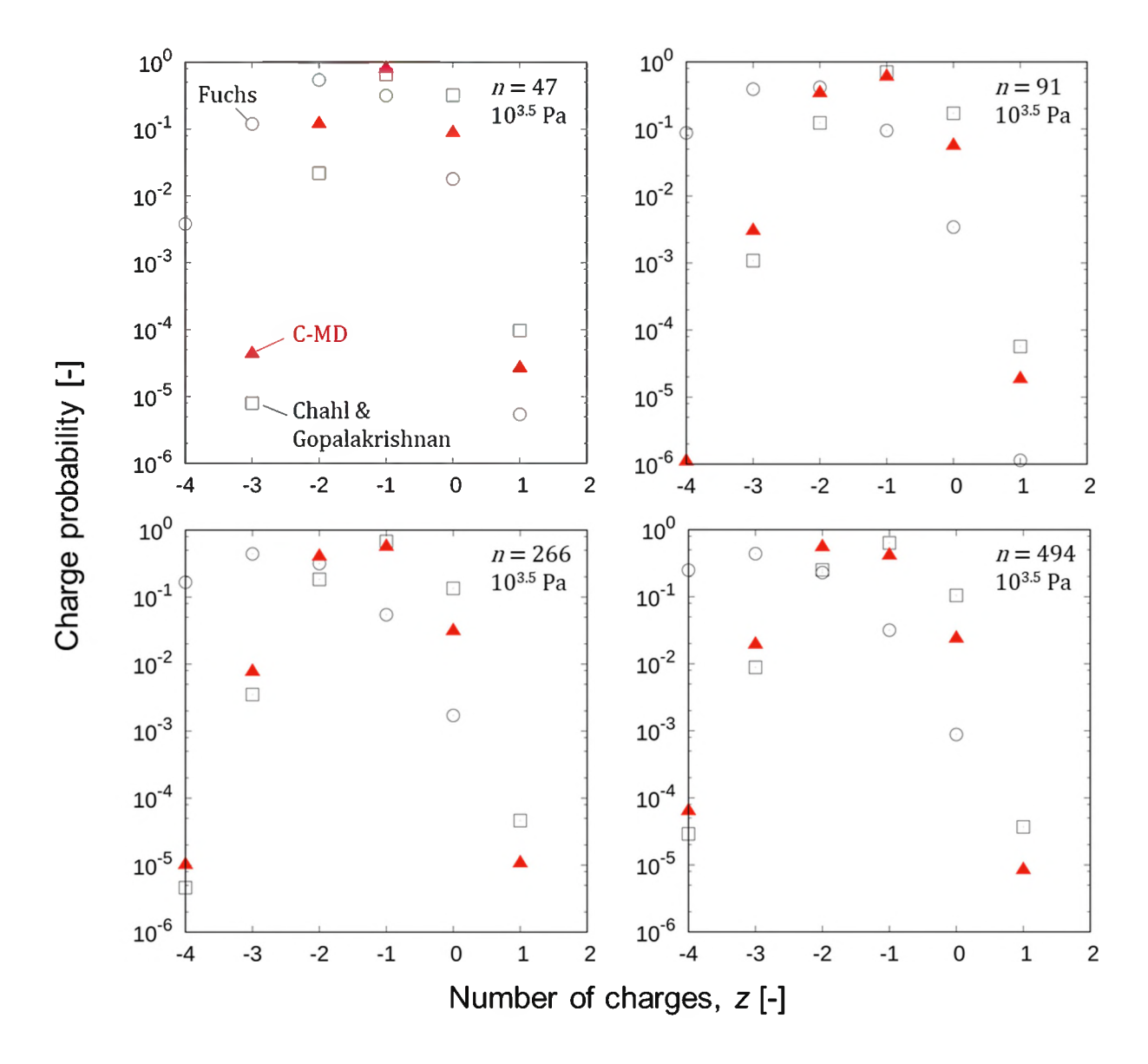


Figure 7. The steady-state charge distributions of Si_n nanoclusters in a non-thermal argon plasma at $10^{3.5}$ Pa and 300 K, with an electron temperature of 2 eV. Circles: Rate coefficients from Fuchs (1963); Square: Rate coefficients from Chahl & Gopalakrishnan (2019), and triangle: C-MD recombination rate coefficients.

Table 2. A summary of the charge distributions calculated at an argon gas pressure of 10^5 Pa for Si_n nanoclusters with an electron temperature of 2 eV. C-MD calculation results are compared to predictions based upon Fuchs (1963) and Chahl & Gopalakrishnan (2019).

		n = 47				n = 91	
z	Fuchs	Chahl & Gopalakrishnan	C-MD	z	Fuchs	Chahl & Gopalakrishnan	C-MD
-5	0.00	0.00	0.00	-5	0.00	0.00	0.00
-4	0.00	0.00	0.00	-4	2.0×10^{-5}	1.1×10^{-5}	$1.5x10^{-5}$
-3	$1.2x10^{-4}$	3.2×10^{-5}	6.9×10^{-5}	-3	$2.7x10^{-3}$	1.6×10^{-3}	$2.2x10^{-3}$
-2	$2.7x10^{-2}$	8.8×10^{-3}	$1.9x10^{-2}$	-2	9.4×10^{-2}	6.2×10^{-2}	8.6x10 ⁻²
-1	$6.3x10^{-1}$	3.2×10^{-1}	5.4x10 ⁻¹	-1	6.6×10^{-1}	5.2×10^{-1}	6.6x10 ⁻¹
0	$3.5x10^{-1}$	6.7×10^{-1}	$4.4x10^{-1}$	0	2.5×10^{-1}	4.2×10^{-1}	2.5x10 ⁻¹
+1	1.1x10 ⁻⁴	2.0×10^{-4}	$1.3x10^{-4}$	+1	8.2×10^{-5}	$1.4x10^{-4}$	8.1x10 ⁻⁵

		n = 266				n = 494	
z	Fuchs	Chahl & Gopalakrishnan	C-MD	z	Fuchs	Chahl & Gopalakrishnan	C-MD
-5	0.00	0.00	0.00	-5	$4.4x10^{-6}$	$3.7x10^{-6}$	3.8x10 ⁻⁶
-4	1.2x10 ⁻⁴	8.7×10^{-5}	$1.2x10^{-4}$	-4	4.5×10^{-4}	3.5×10^{-4}	3.7x10 ⁻⁴
-3	$7.6x10^{-3}$	5.6×10^{-3}	$8.1x10^{-3}$	-3	1.6×10^{-2}	1.3×10^{-2}	1.4×10^{-2}
-2	$1.4x10^{-1}$	1.1×10^{-1}	1.6x10 ⁻¹	-2	$1.9x10^{-1}$	$1.7x10^{-1}$	1.8x10 ⁻¹
-1	$6.3x10^{-1}$	5.6×10^{-1}	$6.2x10^{-1}$	-1	$6.1x10^{-1}$	$5.7x10^{-1}$	6.6x10 ⁻¹
0	$2.2x10^{-1}$	$3.2x10^{-1}$	2.1×10^{-1}	0	1.9x10 ⁻¹	2.5×10^{-1}	1.5x10 ⁻¹
+1	$7.7x10^{-5}$	1.1x10 ⁻⁴	7.2×10^{-5}	+1	6.6x10 ⁻⁵	8.8x10 ⁻⁵	5.3x10 ⁻⁵

Table 3. A summary of the charge distributions calculated at an argon gas pressure of $10^{3.5}$ Pa for Si_n nanoclusters with an electron temperature of 2 eV. C-MD calculation results are compared to predictions based upon Fuchs (1963) and Chahl & Gopalakrishnan (2019).

		n = 47				n = 91	
z	Fuchs	Chahl & Gopalakrishnan	C-MD	z	Fuchs	Chahl & Gopalakrishnan	C-MD
-6	0.00	0.00	0.00	-6	7.3×10^{-5}	0.00	0.00
-5	1.9×10^{-5}	0.00	0.00	-5	$4.9x10^{-3}$	0.00	0.00
-4	$3.8x10^{-3}$	0.00	0.00	-4	$8.7x10^{-2}$	3.9×10^{-7}	1.1×10^{-6}
-3	$1.2x10^{-1}$	8.0×10^{-6}	$4.3x10^{-5}$	-3	$3.9x10^{-1}$	1.1×10^{-3}	$3.0x10^{-3}$
-2	$5.4x10^{-1}$	2.2×10^{-2}	1.2x10 ⁻¹	-2	$4.2x10^{-1}$	1.2×10^{-1}	$3.4x10^{-1}$
-1	$3.2x10^{-1}$	6.6×10^{-1}	$7.9x10^{-1}$	-1	9.5×10^{-2}	7.0×10^{-1}	$6.0x10^{-1}$
0	1.8×10^{-2}	$3.2x10^{-1}$	8.8x10 ⁻²	0	$3.4x10^{-3}$	1.7×10^{-1}	5.6×10^{-2}
+1	$5.4x10^{-6}$	$9.7x10^{-5}$	$2.7x10^{-5}$	+1	1.1x10 ⁻⁶	5.7×10^{-5}	1.9×10^{-5}

	n = 266				n = 494	
z Fuchs	Chahl & Gopalakrishnan	C-MD	z	Fuchs	Chahl & Gopalakrishnan	C-MD
-6 5.8x10 ⁻⁴	0.00	0.00	-6	2.6x10 ⁻³	0.00	0.00
$-5 \ 1.8 \times 10^{-2}$	0.00	0.00	-5	4.5×10^{-2}	0.00	0.00
-4 1.7x10 ⁻¹	4.6×10^{-6}	$1.0x10^{-5}$	-4	2.5x10 ⁻¹	2.9×10^{-5}	6.3×10^{-5}
$-3 \ 4.4 \times 10^{-1}$	3.5×10^{-3}	$7.6x10^{-3}$	-3	$4.4x10^{-1}$	8.8×10^{-3}	1.9×10^{-2}
$-2 \ 3.2 \times 10^{-1}$	1.8×10^{-1}	$4.0x10^{-1}$	-2	$2.3x10^{-1}$	2.5×10^{-1}	5.5×10^{-1}
$-1 5.5 \times 10^{-2}$	6.8×10^{-1}	5.6x10 ⁻¹	-1	$3.2x10^{-2}$	6.4×10^{-1}	4.1x10 ⁻¹
$0 \ 1.7 \times 10^{-3}$	1.4×10^{-1}	$3.1x10^{-2}$	0	$8.8x10^{-4}$	1.1×10^{-1}	2.4×10^{-2}
+1 0.00	4.6×10^{-5}	$1.1x10^{-5}$	+1	0.00	$3.7x10^{-5}$	8.3x10 ⁻⁶

4. CONCLUSIONS

Building upon C-MD calculations for the ion-ion recombination rate (Tamadate, et al., 2020b) and multiply charged-polymer ion charge reduction rate (Tamadate, et al., 2020a), in the present study we extend C-MD calculations to compute the recombination rate for *Si* nanocluster

anions of the form Si_n^z where n = 47,91,266, & 494, z = -1, & -2 with Ar^+ cations at 300 K and pressures from $10^{3.5}$ - $10^{5.5}$ Pa. To deal with the increased computational cost of using many-body potentials (Stillinger & Weber, 1985) for Si atoms within Si_n^z , we further extend the C-MD approach to contain a continuum region, requiring analytical calculations for the recombination rate with inputs from MD calculations, a coarse-grained MD region where the many-potential is not used, and an all atom MD region. Calculation results are intended for application in understanding charge distributions on nanoclusters in non-equilibrium environments.

In total, calculations show that (1) by coarse-graining potentials at large distances, detailed collision rate coefficient calculations are possible in the transition regime in aerosols, (2) C-MD calculations yield rates unique from existing theories, leading to distinct charge distribution predictions in non-thermal plasma conditions, and (3) the fraction of positively charged nanoclusters is negligible in plasma systems, but the fraction of neutral nanoclusters is sufficiently high that neutral-charge nanoparticle-nanocluster collisional growth would be significant.

Finally, we remark that although to date we have only applied C-MD calculations to recombination rate calculations, as noted in Filippov's (1993) description of generalized limiting sphere rate calculations, the C-MD calculation approach can be applied to a wide variety of mass transfer problems in aerosols, including condensation, coagulation, and evaporation. Modifications could also be made to examine transition heat transfer in aerosols (Filippov & Rosner, 2000). We believe that the C-MD approach is uniquely suited to address kinetics in aerosols where transition regime influences (neutral gas collision) manifest, yielding more accurate models of aerosol dynamics. It is similar in complexity to conventional MD calculations, with the main requirement that the domain size (sphere radius) typically needs to be

tuned as part of the calculation procedure. Key to its expanded use will be improvements in computational efficiency; the code used for the present calculations is unparallelized and individual trajectories require seconds-to-minutes to complete.

SUPPORTING INFORMATION

A description of the diffusion coefficient calculation approach and results of a parametric study to optimize the limiting sphere radius are available online.

ACKNOWLEDGEMENTS

This work was supported by US National Science Foundation Award 2002852 and US Department of Energy Award SC0022242.

REFERENCES

- Adachi, M., Kousaka, Y., & Okuyama, K. (1985). Unipolar and bipolar diffusion charging of ultrafine aerosol particles. *J Aerosol Sci*, **16**, 109-123.
- Agarwal, P., & Girshick, S.L. (2012). Sectional modeling of nanoparticle size and charge distributions in dusty plasmas. *Plasma Sources Science and Technology*, **21**, 055023.
- Allen, J.E. (1992). Probe Theory The Orbital Motion Approach. Phys. Scr., 45, 497-503.
- Bürger, P., & Riebel, U. (2020). Electrostatic charging and precipitation of nanoparticles in technical nitrogen: Highly efficient diffusion charging by hot free electrons. *J Aerosol Sci*, **141**, 105495.
- Chahl, H.S., & Gopalakrishnan, R. (2019). High potential, near free molecular regime Coulombic collisions in aerosols and dusty plasmas. *Aerosol Science and Technology*, **53**, 933-957.
- Chen, X., Ghosh, S., Buckley, D.T., Sankaran, R.M., & Hogan, C.J. (2018). Characterization of the State of Nanoparticle Aggregation in Non-equilibrium Plasma Synthesis Systems. *Journal of Physics D: Applied Physics*, **51**, 335203.
- Chen, X., & Hogan, C.J. (2021). Nanoparticle dynamics in the spatial afterglows of nonthermal plasma synthesis reactors. *Chemical Engineering Journal*, **411**, 128383.
- Chen, X., Seto, T., Kortshagen, U.R., & Hogan, C.J. (2020). Size and structural characterization of Si nanocrystal aggregates from a low pressure nonthermal plasma reactor. *Powder Technology*, **373**, 164-173.

- D'yachkov, L.G., Khrapak, A.G., Khrapak, S.A., & Morfill, G.E. (2007). Model of grain charging in collisional plasmas accounting for collisionless layer. *Physics of Plasmas*, **14**, 042102.
- Dahneke, B.E. (1983). Simple Kinetic Theory of Brownian Diffusion in Vapors and Aerosols. In *Theory of Dispersed Multiphase Flow* (Edited Meyer, R.E.), *Theory of Dispersed Multiphase Flow*. Academic Press, City.
- Deser, A., & Kuhne, J. (2021). Unipolar and bipolar aerosol charging as time continuous Markov processes. *J Aerosol Sci*, **158**, 105819.
- Filippov, A.V. (1993). The Charging of Aerosol in the Transition Regime. *J Aerosol Sci*, **24**, 423-436.
- Filippov, A.V., & Rosner, D.E. (2000). Energy transfer between an aerosol particle and gas at high temperature ratios in the Knudsen transition regime. *International Journal of Heat and Mass Transfer*, **43**, 127-138.
- Fuchs, N.A. (1963). On the Stationary Charge Distribution on Aerosol Particles in a Bipolar Ionic Atmosphere. *Geofis. Pura Appl.*, **51**, 185-193.
- Fuchs, N.A. (1964). The mechanics of aerosols (Rev. and enl. ed.). Macmillan, New York,.
- Gallingani, T., Abuyazid, N.H., Colombo, V., Gherardi, M., & Sankaran, R.M. (2020). Online ion mobility spectrometry of nanoparticle formation by non-thermal plasma conversion of metal salts in liquid aerosol droplets. *J Aerosol Sci*, **150**, 105631.
- Gatti, M., & Kortshagen, U. (2008). Analytical model of particle charging in plasmas over a wide range of collisionality. *Physical Review E*, **78**, 046402.
- Girshick, S.L. (2019). Particle nucleation and growth in dusty plasmas: On the importance of charged-neutral interactions. *Journal of Vacuum Science & Technology A*, **38**, 011001.
- Gopalakrishnan, R., & Hogan, C.J. (2011). Determination of the Transition Regime Collision Kernel from Mean First Passage Times. *Aerosol Science and Technology*, **45**, 1499-1509.
- Gopalakrishnan, R., & Hogan, C.J. (2012). Coulomb-Influenced Collisions in Aerosols and Dusty Plasmas. *Physical Review E*, **85**, 026410.
- Gopalakrishnan, R., McMurry, P.H., & Hogan, C.J. (2015). The Bipolar Diffusion Charging of Nanoparticles: A Review and Development of Approaches for Non-Spherical Particles. *Aerosol Science and Technology*, **49**, 1181-1194.
- Goree, J. (1992). Ion Trapping by a Charged Dust Grain in a Plasma. *Physical Review Letters*, **69**, 277-280.
- Hoppel, W.A., & Frick, G.M. (1986). Ion—Aerosol Attachment Coefficients and the Steady-State Charge Distribution on Aerosols in a Bipolar Ion Environment. *Aerosol Science and Technology*, 5, 1-21.
- Husmann, E., Thimsen, E., & Chen, X. (2021). Particle charge distributions in the effluent of a flow-through atmospheric pressure low temperature plasma. *Plasma Sources Science and Technology*, **30**, 075030.
- Khrapak, S.A., Ratynskaia, S.V., Zobnin, A.V., Usachev, A.D., Yaroshenko, V.V., Thoma, M.H., Kretschmer, M., Höfner, H., Morfill, G.E., Petrov, O.F., & Fortov, V.E. (2005). Particle charge in the bulk of gas discharges. *Physical Review E*, **72**, 016406.
- Kortshagen, U. (2016). Nonthermal Plasma Synthesis of Nanocrystals: Fundamentals, Applications, and Future Research Needs. *Plasma Chemistry and Plasma Processing*, **36**, 73-84.

- Kortshagen, U.R., Sankaran, R.M., Pereira, R.N., Girshick, S.L., Wu, J.J., & Aydil, E.S. (2016). Nonthermal Plasma Synthesis of Nanocrystals: Fundamental Principles, Materials, and Applications. *Chemical Reviews*, **116**, 11061-11127.
- Kramer, N.J., Anthony, R.J., Mamunuru, M., Aydil, E.S., & Kortshagen, U.R. (2014). Plasma-induced crystallization of silicon nanoparticles. *Journal of Physics D-Applied Physics*, 47, 075202.
- Langevin, P. (1903). Recombination et Mobilites des Ions dans les Gaz. *Annales de chimie et de physique*, **28**, 433-530.
- Lanham, S.J., Polito, J., Shi, X., Elvati, P., Violi, A., & Kushner, M.J. (2021). Scaling of silicon nanoparticle growth in low temperature flowing plasmas. *Journal of Applied Physics*, **130**, 163302.
- Larriba-Andaluz, C., & Carbone, F. (2021). The size-mobility relationship of ions, aerosols, and other charged particle matter. *J Aerosol Sci*, **151**, 105659.
- Larriba-Andaluz, C., & Prell, J.S. (2020). Fundamentals of ion mobility in the free molecular regime. Interlacing the past, present and future of ion mobility calculations. *International Reviews in Physical Chemistry*, **39**, 569-623.
- Le Picard, R., Markosyan, A.H., Porter, D.H., Girshick, S.L., & Kushner, M.J. (2016). Synthesis of Silicon Nanoparticles in Nonthermal Capacitively-Coupled Flowing Plasmas: Processes and Transport. *Plasma Chemistry and Plasma Processing*, **36**, 941-972.
- Lee, H.S., & Johnsen, R. (1989). Ion-ion recombination studies in ambient helium and argon at atmospheric densities. *The Journal of Chemical Physics*, **90**, 6328-6334.
- Li, L., Chahl, H.S., & Gopalakrishnan, R. (2020). Comparison of the predictions of Langevin Dynamics-based diffusion charging collision kernel models with canonical experiments. *J Aerosol Sci*, **140**, 105481.
- Li, L., & Gopalakrishnan, R. (2020). An experimentally validated model of diffusion charging of arbitrary shaped aerosol particles. *J Aerosol Sci*, 105678.
- Loeb, L.B. (1937). Theory of Recombination of Ions Over an Extended Pressure Range. *Physical Review*, **51**, 1110-1111.
- Loeb, L.B., & Marshall, L.C. (1929). The theory of recombination of gaseous ions. *Journal of the Franklin Institute*, **208**, 371-388.
- Madson, J.M., & Oskam, H.J. (1967). Mobility of Argon ions in argon. *Physics Letters A*, **25**, 407-408.
- Mamunuru, M., Le Picard, R., Sakiyama, Y., & Girshick, S.L. (2017). The Existence of Nonnegatively Charged Dust Particles in Nonthermal Plasmas. *Plasma Chemistry and Plasma Processing*, **37**, 701-715.
- Mangolini, L., & Kortshagen, U. (2009). Selective nanoparticle heating: Another form of nonequilibrium in dusty plasmas. *Physical Review E*, **79**, 026405.
- Mangolini, L., Thimsen, E., & Kortshagen, U. (2005). High-yield plasma synthesis of luminescent silicon nanocrystals. *Nano Letters*, **5**, 655-659.
- Mariotti, D., & Sankaran, R.M. (2010). Microplasmas for nanomaterials synthesis. *Journal of Physics D-Applied Physics*, **43**.
- Marlow, W.H., & Brock, J.R. (1975). Calculations of bipolar charging of aerosols. *Journal of Colloid and Interface Science*, **51**, 23-31.
- Marquard, A. (2007). Unipolar Field and Diffusion Charging in the Transition Regime—Part I: A 2-D Limiting-Sphere Model. *Aerosol Science and Technology*, **41**, 597-610.

- Mason, E.A., & McDaniel, E.W. (1988). Transport Properties of Ions in Gases. Wiley, New York.
- Matsoukas, T., & Russell, M. (1995). Particle charging in low pressure plasmas. *Journal of Applied Physics*, 77, 4285-4292.
- Mott-Smith, H.M., & Langmuir, I. (1926). The Theory of Collectors in Gaseous Discharges. *Physical Review*, **28**, 727-763.
- Natanson, G. (1960). On the theory of charging of amicroscopic aerosol particles resulting from the capture of gaseous ions. *Soviet Physics Technical Physics*, **5**, 538-551.
- Ravi, L., & Girshick, S.L. (2009). Coagulation of nanoparticles in a plasma. *Physical Review E*, 79
- Santos, B., Cacot, L., Boucher, C., & Vidal, F. (2019). Electrostatic enhancement factor for the coagulation of silicon nanoparticles in low-temperature plasmas. *Plasma Sources Science and Technology*, **28**, 045002.
- Sawyer, W.J., & Hart, A.J. (2021). High-yield microplasma synthesis of monodisperse sub-3 nm diameter metal nanoparticles explained by a charge-mediated formation mechanism. *J Aerosol Sci*, 105915.
- Sharma, G., Abuyazid, N., Dhawan, S., Kshirsagar, S., Sankaran, R.M., & Biswas, P. (2020). Characterization of particle charging in low-temperature, atmospheric-pressure, flow-through plasmas. *Journal of Physics D: Applied Physics*, **53**, 245204.
- Sipkens, T.A., & Daun, K.J. (2018). Effect of Surface Interatomic Potential on Thermal Accommodation Coefficients Derived from Molecular Dynamics. *The Journal of Physical Chemistry C*, **122**, 20431-20443.
- Stillinger, F.H., & Weber, T.A. (1985). Computer simulation of local order in condensed phases of silicon. *Physical Review B*, **31**, 5262-5271.
- Stommel, Y.G., & Riebel, U. (2007). Comment on the Calculation of the Steady-State Charge Distribution on Aerosols < 100 nm by Three Body Trapping Method in a Bipolar Ion Environment. *Aerosol Science and Technology*, **41**, 840-847.
- Suresh, V., Li, L., Redmond Go Felipe, J., & Gopalakrishnan, R. (2021). Modeling nanoparticle charge distribution in the afterglow of non-thermal plasmas and comparison with measurements. *Journal of Physics D: Applied Physics*, **54**, 275205.
- Tamadate, T., Higashi, H., Hogan, C.J., & Seto, T. (2020a). The charge reduction rate for multiply charged polymer ions via ion—ion recombination at atmospheric pressure. *Physical Chemistry Chemical Physics*, **22**, 25215-25226.
- Tamadate, T., Higashi, H., Seto, T., & Hogan, C.J. (2020b). Calculation of the ion–ion recombination rate coefficient via a hybrid continuum-molecular dynamics approach. *The Journal of Chemical Physics*, **152**, 094306.
- Thomson, J.J. (1924). XXIX. Recombination of gaseous ions, the chemical combination of gases, and monomolecular reactions. *The London, Edinburgh, and Dublin Philosophical Magazine and Journal of Science*, **47**, 337-378.
- Uner, N.B., Niedzwiedzki, D.M., & Thimsen, E. (2019). Nonequilibrium Plasma Aerotaxy of InN Nanocrystals and Their Photonic Properties. *The Journal of Physical Chemistry C*, **123**, 30613-30622.
- Uner, N.B., & Thimsen, E. (2017). In-Flight Size Focusing of Aerosols by a Low Temperature Plasma. *The Journal of Physical Chemistry C*, **121**, 12936-12944.
- Uner, N.B., & Thimsen, E. (2018). Low temperature plasma as a means to transform nanoparticle atomic structure. *Plasma Sources Science and Technology*, **27**, 074005.

- Wiedensohler, A. (1988). An approximation of the bipolar charge distribution for particles in the submicron size range. *J Aerosol Sci*, **19**, 387-389.
- Wright, P.G. (1960). On the Discontinuity Involved in Diffusion Across an Interface (The Delta of Fuchs). *Discussions of the Faraday Society*, **30**, 100-112.
- Yang, H., Drossinos, Y., & Hogan, C.J. (2019). Excess thermal energy and latent heat in nanocluster collisional growth. *The Journal of Chemical Physics*, **151**, 224304.
- Yang, H., Song, G., & Hogan, C.J. (2022). A molecular dynamics study of collisional heat transfer to nanoclusters in the gas phase. *J Aerosol Sci*, **159**, 105891.